Mechanical Scission of Perfluoropolyethers

T. E. KARIS,* V. J. NOVOTNY, and R. D. JOHNSON

IBM Research Division, Almaden Research Center, 650 Harry Road, San Jose, California 95120-6099

SYNOPSIS

Mechanical scission of two typical perfluoropolyethers was investigated: Y, a copolymer of $-CF(CF_3)CF_2O-$, $-CF_2O-$, and $-CF(CF_3)O-$, and Z, a copolymer of $-(CF_2)_nO-$, with $n = 1, 2, 3, 4$. Undiluted polymers were subjected to prolonged shearing in a media mill with ZrO_2 particles. A chemical extraction of the polar ZrO_2 particles was carried out to collect adsorbed polar scission products. Mechanochemical scission products from both the Y and Z fluorocarbon polymers were identified by ^{19}F-NMR. A significant amount of $CF_3CO_2^-$ was present after the milling and the primary functional groups formed at scissioned chain ends were $-CO_2^-$. A hydrodynamic expression was derived and the maximum extension rate was estimated to be in the range of $5 \times 10^6\ s^{-1}$. Initial degrees of polymerization were between 20 and 200, well below levels for which flow-induced scission is expected to occur. Final degrees of polymerization were less than 10, and the scission was noncentral and nonrandom in both polymers. © 1993 John Wiley & Sons, Inc.

INTRODUCTION

Perfluoropolyethers have come into widespread use for a variety of applications requiring exceptional stability, inertness, low surface energy, and low vapor pressure. These applications include vacuum pump fluids, high shear strength lubricants, and magnetic recording disk and tape lubricants. Even though these polymers are highly thermally stable, a number of studies have reported conditions that produce significant decomposition. These studies have focused on the thermal catalytic decomposition.[1-5] Scission of perfluoropolyethers has also been observed during lubricated sliding of stainless steel[6] and at the head-disk interface in magnetic recording systems.[7] The decomposition on steel was attributed to chemical reaction at active metal sites due to asperity wear. Scission mechanisms at the head-disk interface might include mechanical, thermal, catalytic, and triboelectric processes.

We consider two typical molecular structures[1,8]: Y, a copolymer of $-CF(CF_3)CF_2O-$, $-CF_2O-$, and $-CF(CF_3)O-$ groups, and Z, a copolymer of $-(CF_2)_nO-$ groups, with $n = 1, 2, 3, 4$. In the presence of a Lewis acid catalyst, such as $AlCl_3$, these polymers decompose at a rate that depends on their molecular structure.[1-5] The Y structure is more stable than the Z on $AlCl_3$ because steric hinderance by the $-CF_3$ in the $-CF(CF_3)CF_2O-$ group of the Y polymer suppresses disproportionation by limiting access to catalytic sites.[3-5].

In general, mechanochemical scission of polymers is possible under the extremely high shear rates (up to $10^{10}\ s^{-1}$) encountered during sliding in boundary-lubricated systems. It is well known that polymer chains can be severed by purely mechanical forces encountered in high-shear situations. One recent study[9,10] subjected high molecular weight polymer chains in solution to an extensional flow field that is intense enough to overcome the intramolecular bond strength of the polymers. The extensional flow is produced by impinging jets of the polymer solution or by a crossed slot flow cell, both of which generate extensional flow at the stagnation point. Changes in the molecular weight distribution of the polymers are interpreted by postulating that the chains are completely uncoiled at some critical extension rate $\dot{\gamma}_c$ and that the chains are fractured at the extension rate $\dot{\gamma}_f > \dot{\gamma}_c$.

In this model, the scission can occur only when the chains are fully uncoiled. Hydrodynamic theory suggests that the minimum extension rate necessary

* To whom correspondence should be addressed.

Journal of Applied Polymer Science, Vol. 50, 1357–1368 (1993)
 CCC 0021-8995/93/081357-12

to produce scission is proportional to the inverse of polymer molecular weight, M:

$$\dot{\gamma}_f \propto \frac{1}{M^b} \tag{1}$$

where $b = 2$ for steady extensional flow and $b \approx 1$ for transient extensional flow.[11,12] A thermally activated barrier-to-scission model[9] predicts how the minimum extension rate necessary to produce scission depends on the polymer properties:

$$\dot{\gamma}_f \propto \frac{U_0}{a(Nl)^2} \tag{2}$$

in which U_0 is the bond dissociation energy; a, the (stretched) bond length; N, the number of monomer units in the polymer; and l, the equilibrium bond length. Within these models, the distributed tension along the uncoiled polymer results in the largest forces at the center of the chain, thus predicting that chains can break only at the center in a steady extensional flow. This is a consequence of how the force on the uncoiled chain is calculated. The opposing hydrodynamic forces on the segments are integrated from the center of the chain toward the ends.

One implication of this model is that, for a given bond dissociation energy, there is a lower limit of molecular weight below which chain scission cannot occur at a physically realizable extension rate [see eqs. (1) and (2)]. For example, no scission was detected during the Couette flow of a polyisobutylene solution[13] with molecular weight below 5×10^4 and in cold milling of undiluted polyisobutylene[14] with molecular weight below 4×10^5. In general, there seems to be a limiting molecular weight below which no scission was detected in various flow fields in both polymer solutions[15–17] and in undiluted polymer.[14,18]

There is also the possibility that chain scission may occur at points other than at the chain center. Noncentral scission may be produced by turbulent flow[17] or in extensional flows when entanglements are present in undiluted polymer.[14] Theory for polymer scission in turbulent flow has not yet been developed.

The scission is the cleavage of bonds in the polymer backbone. One of three possible reactions occur once a bond is broken.[19] Homolytic cleavage can be represented as

$$P_{n+m} \rightarrow P_n^{\bullet} + P_m^{\bullet} \tag{3}$$

where $P^{\bullet}$ signifies a product radical. Heterolytic cleavage is

$$P_{n+m} \rightarrow P_n^{\bullet} + P_m^{\bullet} \rightarrow P_n^{\bullet} + e^- + P_m^{\bullet} - e^- \rightarrow P_n^- + P_m^+ \tag{4}$$

and disproportionation is

$$P_{n+m} \rightarrow P_n + P_m \tag{5}$$

The occurrence of each type of reaction is determined by the chemical composition of the polymer. In this study, we investigate perfluoropolyether scission by subjecting the bulk polymer to intense hydrodynamic forces in a media mill.

EXPERIMENTAL

Materials

Two perfluoropolyether random block copolymers with different molecular structure[1] were investigated. The Y polymer with the CF_3 side groups has the structure

Backbone

$$\{-[CF(CF_3)CF_2O]_m-[CF_2O]_n-[CF(CF_3)O]_p-\}_{DP_n}$$

Ends

$$-[OCF_3]_u$$
$$-[OCF_2CF_3]_v$$
$$-[OCF_2CF_2CF_3]_w$$
$$-[OCF(CF_3)CO_2^-]_x$$
$$-[OCF(CF_3)CF_3]_y$$

The linear Z polymer is described as follows:

Backbone

$$\{-[CF_2O]_m-[CF_2CF_2O]_n-[CF_2CF_2CF_2O]_p-[CF_2CF_2CF_2CF_2O]_q-\}_{DP_n}$$

Ends

$$-[OCF_3]_x$$
$$-[OCF_2CO_2^-]_y$$

The acid end groups and

Trifluoroacetic Acid

$CF_3CO_2^-$

are absent in the initial polymers and will be discussed later. The initial composition is given in Table I. M_n is the number-average molecular weight and DP_n is the number-average degree of polymerization.

The viscosity of the Y is 2.5 Pa-s and that of the Z is 0.42 Pa-s at 25°C. The Z has a substantially lower bulk viscosity than that of Y, because Z is a linear polymer, whereas Y has a CF_3 side group that increases its intermolecular friction coefficient.

Apparatus and Procedure

Milling

Samples of each polymer were subjected to prolonged shearing in an Eiger mini media mill (Eiger Machinery, Inc., Chicago, IL, Model V.S.E. Mini Motormill, 1000 W). The volumetric capacity of the mill chamber was approximately 50 mL. The mill charge was 46 g of polymer and 142 g of media. Fluid was recirculated from the exit port by directing the discharge tube back into the charging funnel (Fig. 1). The mill jacket was cooled with water to prevent frictional heating. The milling media were ZrO_2 particles with an average diameter of 0.6 mm. Scanning electron micrographs of the milling media in Figure 2 show the roughness and porosity of these particles. The mill was run at 2.6 Krpm for 3 h with the Z polymer, and for 3 h and 6 h (using separate charges) for the Y polymer. Between each polymer charge, the mill chamber was thoroughly cleaned and fresh media was installed.

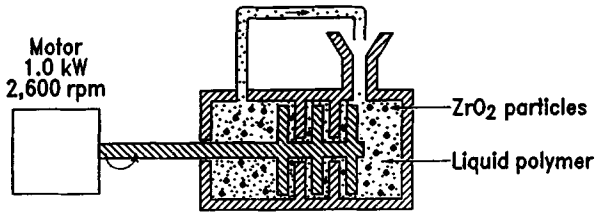

Figure 1 Schematic representation of the polymer milling apparatus.

Extraction of Scission Products

In all cases, the liquid polymer was separated from the media by washing with 1,1,2-trichlorotrifluoroethane (FR, 99.99% purity). The polymer, dissolved in the FR, contained ZrO_2 media debris. This was removed by successive filtration through 0.45 and then 0.05 μm Millipore filters. FR was then removed from the filtered solution by evaporation for at least 48 h at ambient conditions. The FR washed media were extracted with 2,2,2-trifluoroethanol (TFE, 99.5+% purity), which is polar-solvent compared to FR, in order to remove degradation products that were insoluble in the FR. The TFE was evaporated and the residue was dissolved in deuterated methanol for NMR analysis.

Characterization of Scission Products

^{19}F-NMR spectra were obtained on an IBM Instruments AF/300, operating at a frequency of 282 MHz. The ^{19}F chemical shifts for the spectra were referenced to internal $CFCl_3$. Typically, 20,000 scans

Table I Composition of the Initial Polymers and Extracts after Milling

	Y Polymer			
	m/n/p (%)	*u/v/w/x/y* (%)	DP_n	M_n
Initial	95.7/3.3/1.0	33.9/53.8/12.3/0/0	22	3,900
Milled 3 h	100/0/0	0/0/0/63/37	3	850
Milled 6 h	100/0/0	0/0/0/100/0	3	850
	Z Polymer			
	m/n/p/q (%)	*x/y* (%)	DP_n	M_n
Initial	61.2/34.9/3.0/0.9	100/0	200	17,000
Milled 3 h	30.7/65.9/1.0/2.4	36/64	6	800

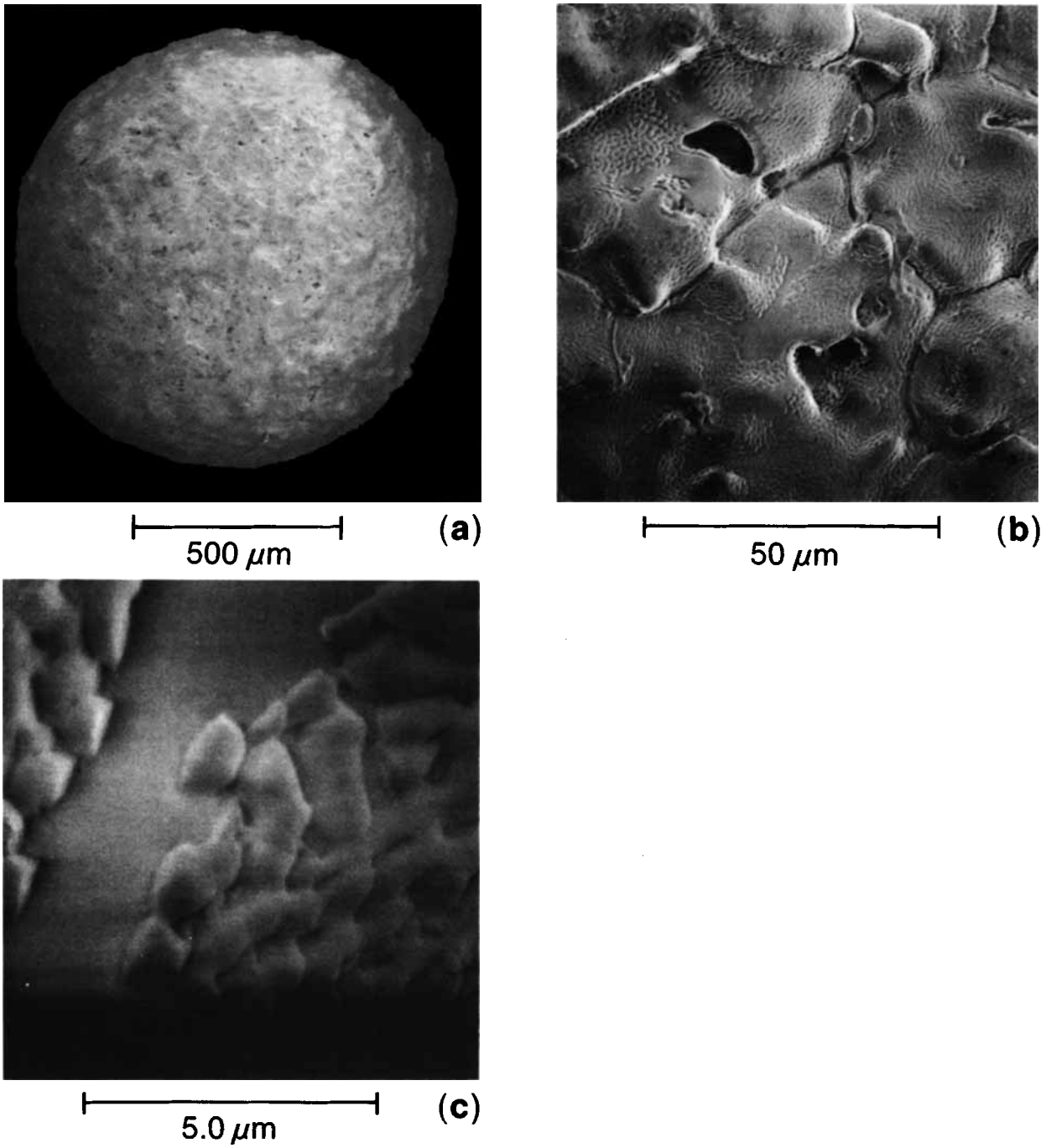

Figure 2 Scanning electron micrographs of the ZrO_2 milling media particles.

were collected over a chemical-shift range of 150 ppm that was digitized into 64,000 data points; care was taken to avoid saturation of the resonances.

RESULTS

The initial tests were carried out on the bulk of the polymer after milling once the media debris was removed by filtration. There was no detectable change in molecular weight or viscosity by cone and plate rheometry, gel permeation chromatography, NMR, or Fourier transform infrared spectroscopy. Little chain scission was expected, since the DP_n of the initial polymer chains for the Y and Z polymers was less than the minimum of 1000–7000 (Refs. 13–18) needed for mechanical scission as reported in the literature. It was possible that scission products were

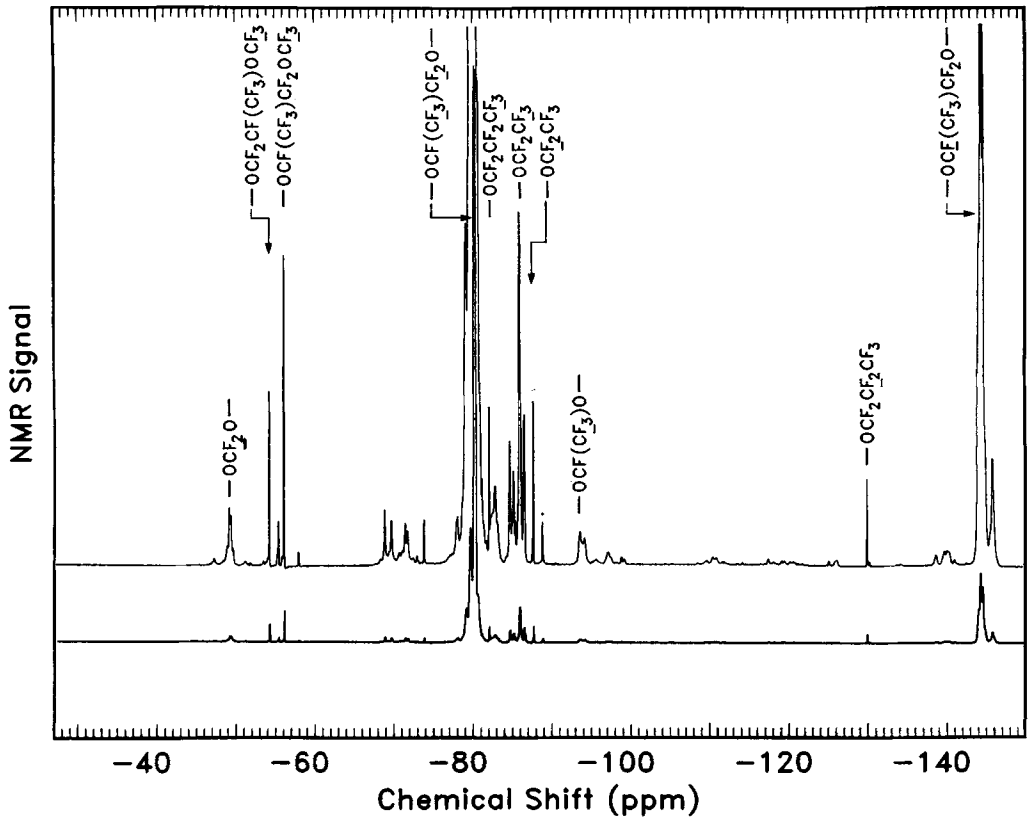

Figure 3 ^{19}F-NMR spectra of the initial Y polymer.

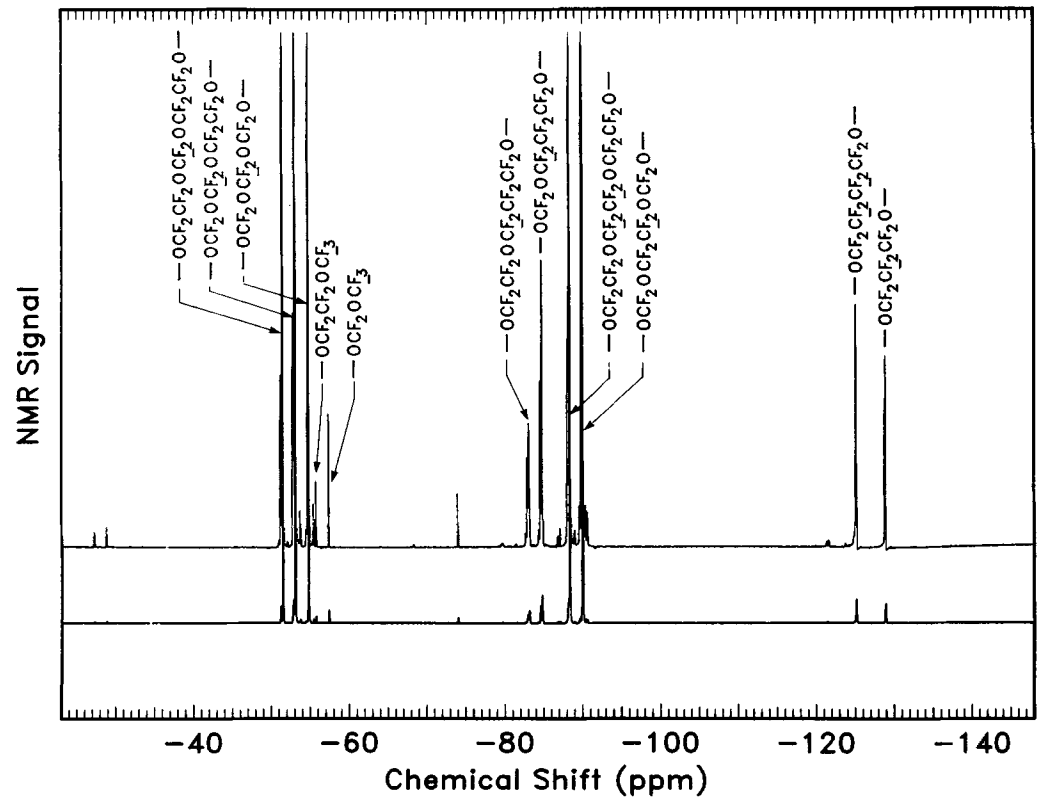

Figure 4 ^{19}F-NMR spectra of the initial Z polymer.

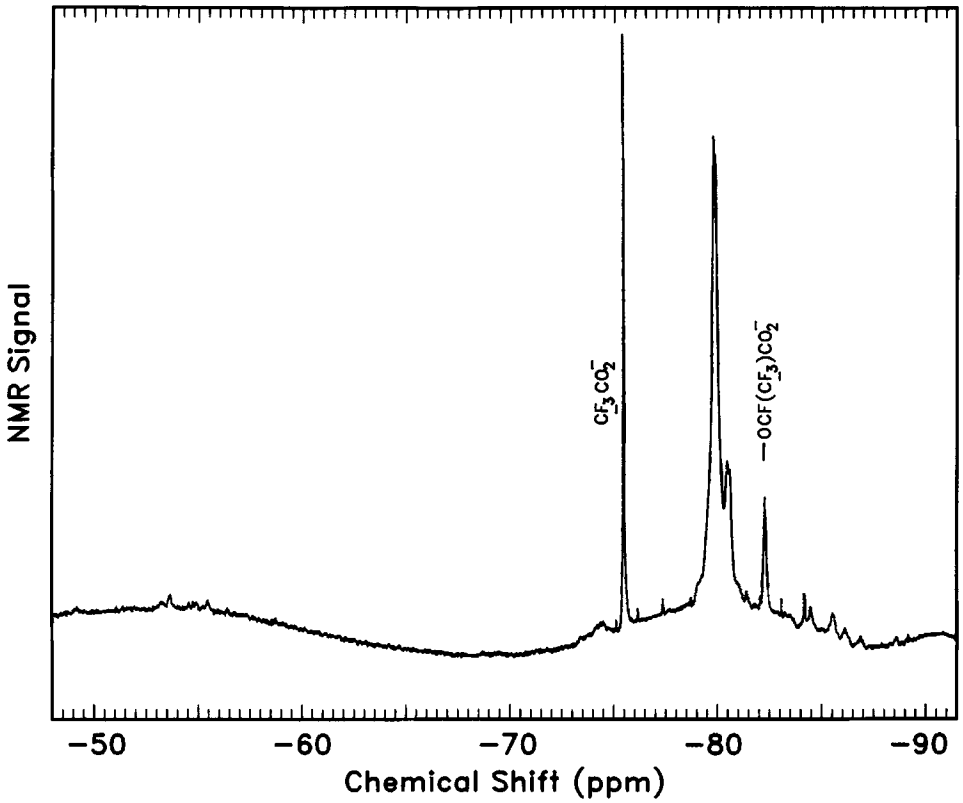

Figure 5 ^{19}F-NMR spectrum of the Y polymer after 3 h milling. New NMR peaks are labeled.

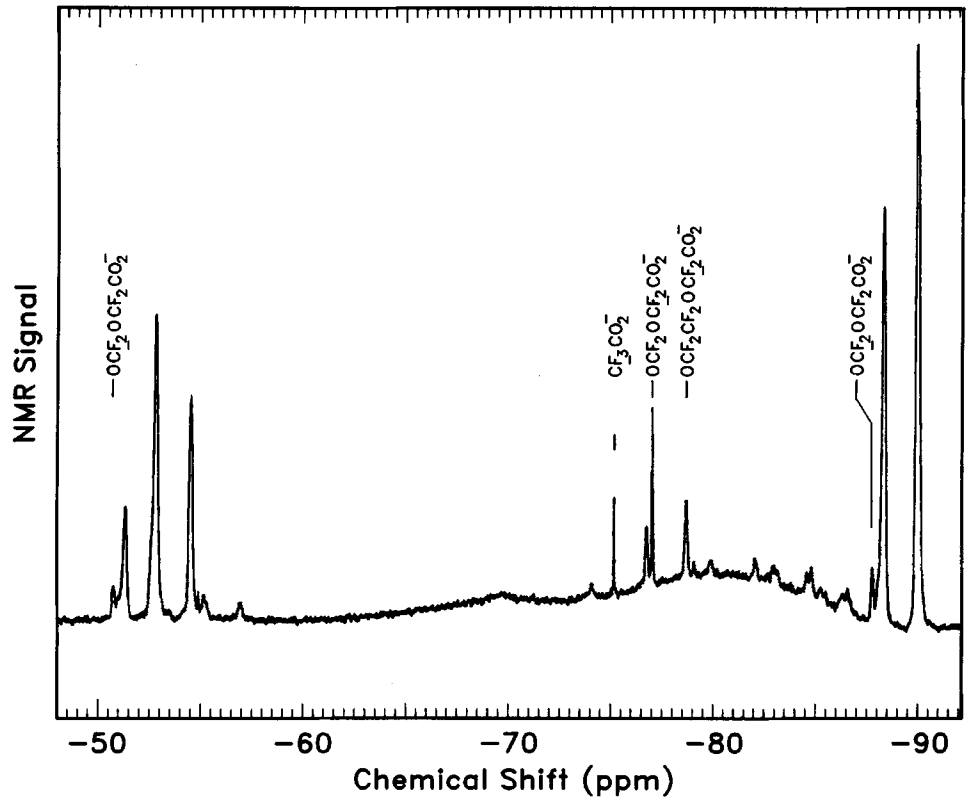

Figure 6 ^{19}F-NMR spectrum of the Z polymer after 3 h milling. New NMR peaks are labeled.

Table II NMR Peak Assignments for Y Polymer

Peak Assignment	Chemical Shift (ppm)	Relative Peak Areas		
		Initial	3 h	6 h
—$O\underline{C}F_2O$—	−49.0	0.014	≃ 0.00	≃ 0.00
—$OCF_2\underline{C}F(CF_3)O\underline{C}F_3$	−53.5	0.009	≃ 0.00	≃ 0.00
—$OCF(CF_3)\underline{C}F_2O\underline{C}F_3$	−55.5	0.010	≃ 0.00	≈ 0.00
$C\underline{F}_3CO_2^-$	−75.5	0.000	> 2.30	> 2.40
—$OCF(C\underline{F}_3)C\underline{F}_2O$—	−80.0	1.000	1.00	1.00
—$OCF(C\underline{F}_3)C\underline{F}_3$	−81.0	0.000	0.29	≃ 0.00
—$OCF_2CF_2C\underline{F}_3$	−82.0	0.007	≃ 0.00	≃ 0.00
—$OCF(C\underline{F}_3)CO_2^-$	−82.2	0.000	0.25	0.37
—$OCF_2C\underline{F}_3$	−87.0	0.031	≃ 0.00	≃ 0.00
—$OC\underline{F}_2CF_3$	−88.0	0.021	≃ 0.00	≃ 0.00
—$OCF(C\underline{F}_3)O$—	−93.0	0.006	≃ 0.00	≃ 0.00
—$OCF_2C\underline{F}_2CF_3$	−130.0	0.005	≃ 0.00	≃ 0.00
—$OC\underline{F}(CF_3)CF_2O$—	−144.0	0.200	0.20	0.20

at too low a concentration in the bulk or could have adsorbed on the polar ZrO_2 media particles. To examine the second possibility, the media were extracted and the extract was examined by ^{19}F-NMR. The NMR spectra of the initial polymers and the extracts are shown in Figures 3–6. Integrated areas for the peaks are listed in Tables II and III.

The composition, M_n, and DP_n were calculated from the relative NMR peak areas of backbone groups, a_{bi}, and end groups, a_{ei}. For the Y polymer, the —$OCF(C\underline{F}_3)C\underline{F}_2O$— peak was assigned an area of 1.0, and for the Z polymer, the —OCF_2O-$C\underline{F}_2C\underline{F}_2OCF_2O$— peak was assigned an area of 1.0. The a_{bi} and a_{ei}, normalized by the number of responding F atoms in each subunit, are denoted $\tilde{a}_{bi}$ and $\tilde{a}_{ei}$. For example, consider the —$O\underline{C}F_2O$— relative peak areas in Table III. There are two F atoms responding, so that the relative amount of these groups present is then $\tilde{a}_{bi} = (0.2 + 0.6 + 0.63)/2 = 0.715$. This calculation is carried out for each back-

Table III NMR Peak Assignments for the Z Polymer

Peak Assignment	Chemical Shift (ppm)	Relative Peak Areas	
		Initial	3 h
—$O\underline{C}F_2OCF_2CO_2^-$	−50.9	0.000	0.250
—$OCF_2CF_2O\underline{C}F_2OCF_2CF_2O$—	−51.5	0.200	0.140
—$OCF_2O\underline{C}F_2OCF_2CF_2O$—	−53.1	0.600	0.170
—$OCF_2O\underline{C}F_2OCF_2O$—	−54.8	0.630	0.098
—$OCF_2CF_2O\underline{C}F_3$	−55.4	0.012	0.120
—$OCF_2O\underline{C}F_3$	−57.1	0.023	0.130
$C\underline{F}_3CO_2^-$	−75.3	0.000	0.072
—$OCF_2O\underline{C}F_2CO_2^-$	−77.0	0.000	0.250
—$OCF_2CF_2O\underline{C}F_2CO_2^-$	−79.0	0.000	0.050
—$OCF_2CF_2O\underline{C}F_2CF_2CF_2O$—	−83.2	0.021	≃ 0.000
—$OCF_2O\underline{C}F_2CF_2CF_2O$—	−84.9	0.050	≃ 0.000
—$OCF_2C\underline{F}_2OCF_2CO_2^-$	−88.0	0.000	0.050
—$OCF_2CF_2O\underline{C}F_2C\underline{F}_2OCF_2CF_2O$—	−88.5	0.630	0.750
—$OCF_2O\underline{C}F_2C\underline{F}_2OCF_2O$—	−90.1	1.000	1.000
—$OCF_2C\underline{F}_2C\underline{F}_2CF_2O$—	−125.5	0.042	0.063
—$OCF_2C\underline{F}_2CF_2O$—	−129.2	0.033	0.014

bone and end group. The mol percent composition of the backbone is then calculated from the $\tilde{a}_{bi}$. The mol percent of group i in the backbone is

$$\tilde{a}_{bi}(\%) = \tilde{a}_{bi} \times 100 \Big/ \sum_{j=1}^{N_b} \tilde{a}_{bj} \qquad (6)$$

where N_b is the number of unique backbone groups. An analogous equation is used to calculate the mol percent of the end groups. The percent composition among the backbone groups is given in the second column of Table I, and the percent composition among the end groups is in the third column of Table I.

The $\tilde{a}_{bi}$ and $\tilde{a}_{ei}$ must then be adjusted by the number of end groups to calculate the M_n and DP_n. Since there are two end groups per chain,

$$M_n = \frac{2 \times \left\{ \sum_{i=1}^{N_e} M_{ei}\tilde{a}_{ei} + \sum_{i=1}^{N_b} M_{bi}\tilde{a}_{bi} \right\}}{\sum_{i=1}^{N_e} \tilde{a}_{ei}} \qquad (7)$$

and

$$DP_n = \frac{2 \times \sum_{i=1}^{N_b} \tilde{a}_{bi}}{\sum_{i=1}^{N_e} \tilde{a}_{ei}} \qquad (8)$$

where N_e is the number of unique end groups and M_{bi} and M_{ei} are the molecular weights of the respective subgroups. The M_n and DP_n are given in the fourth and fifth columns of Table I, respectively.

To test the possibility that the ZrO_2 media were only concentrating fragments already present in the initial polymer remaining from the polymerization reaction, 60 g of Y polymer were placed on 38 g of the media for 48 h without any milling and the media were extracted the same way as in the milling test. After 140,000 NMR scans, a small amount of material corresponding to the initial Y polymer was detected. The amount of —OCF(CF$_3$)CF$_2$O— relative to that in the extract from the Y polymer after milling was determined by comparing the —OCF(CF$_3$)CF$_2$O— group signal height with the background noise level, normalized for the number of scans N (noise $\propto 1/\sqrt{N}$). Taking into account the larger polymer/media weight ratio between the control test and the milling test, there was at least 50 times more of —OCF(CF$_3$)CF$_2$O— in the extract following milling than in the control. In addition, acid end groups were not detected in the control. Thus, the fragments detected in the extract after milling were produced by the mechanical energy input to the polymer/media system during the milling. The small amount of —OCF(CF$_3$)CF$_2$O— detected in the control test is attributed to incomplete extraction of the original polymer from pores within the ZrO_2 media particles during the FR rinse.

To study the possibility that the scission products observed during milling are produced by a thermal/catalytic mechanism, Y and Z polymer samples were combined with ZrO_2 media and held at 250°C for 34 h. Any scission products were examined by NMR as in the milling test and no such products were detected. If any thermal/catalytic scission occurred during milling, the temperature then would have to be much greater than 250°C, which is normally sufficient to degrade 96% of the Z polymer on Al_2O_3 within less than 2 h.[3,5]

DISCUSSION

Strain Rate during Milling

Milling is usually characterized by the particle-size reduction ratio, bond work index, grinding efficiency, and energy coefficient.[20] These are semiempirical parameters that relate the macroscopically observable quantities such as power input, particle-size reduction, and the mill geometry. The macroscopic description of milling is inadequate for interpretation of the current polymer chain scission test. The flow field near the interface between two media particles in close proximity can, in principle, be used to obtain the local extension rate. The following analysis is meant to provide an order of magnitude estimate for the maximum extension rate. Polymer scission is dependent on the maximum extension rate; therefore, only the region of closest approach between two colliding particles is considered. A cylindrical coordinate system as shown in Figure 7 is employed, with the origin at the central point between two spheres. The minimum separation is $2h_0$ at $r = 0$. The distance between the surfaces of the two spheres, $2h$, is a function of radial distance from the origin, r. When the gap is much less than the radius a ($h \ll a$), the half-width of the spacing between the surfaces of the two spheres is

$$h(r) \approx h_0 + \frac{r^2}{2a} \qquad (9)$$

The velocity field between the two spheres near the

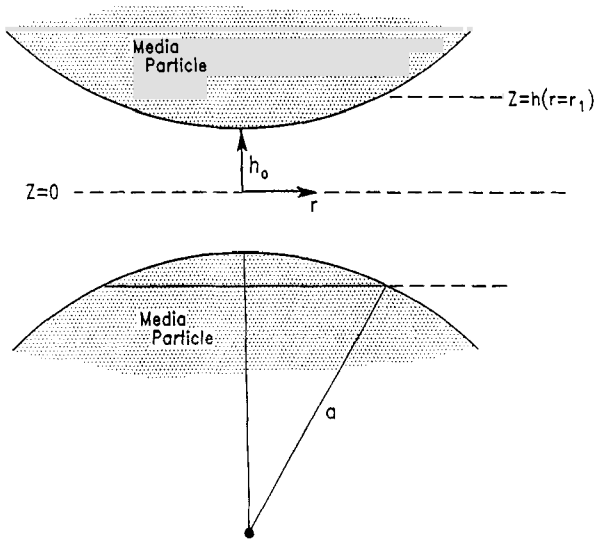

Figure 7 A schematic of the coordinate system used to model the flow between two closely approaching media particles.

point of closest proximity is approximated by a squeezing flow of a Newtonian fluid between two parallel plates[21]:

$$v_r = -\frac{3}{4}\left(\frac{h'}{h}\right) r\left[1 - \left(\frac{z}{h}\right)^2\right] \qquad (10)$$

where v_r is the fluid velocity in the radial direction, $h' = dh/dt$ is the relative velocity between the two solid surfaces, and h is given by eq. (9). The molecular weight of these polymers is relatively low; thus, Newtonian behavior is expected up to very high shear or extension rates.

The velocity from eq. (10) and the known power input to the mill are used to estimate the extensional flow rate in the gap between two media particles as follows: The viscous dissipation in one region of near contact between two media particles is

$$\frac{Q'}{N} = \frac{1}{2}\eta \int_0^{2\pi}\int_0^{\infty}\int_{-h}^{h} \dot{\underline{\underline{\gamma}}} : \dot{\underline{\underline{\gamma}}}\, dz\, r dr\, d\theta \qquad (11)$$

where $\dot{\underline{\underline{\gamma}}}$ is the rate of strain tensor; Q', the energy dissipation or power input into the mill; η, the viscosity; N, the number of particle–particle interfaces in the mill, and $\dot{\underline{\underline{\gamma}}} : \dot{\underline{\underline{\gamma}}} = \sum_i \sum_j \dot{\gamma}_{ij}\dot{\gamma}_{ij}$, where $i, j = r, z, \theta$. $\dot{\gamma}_{rr} = 2(\partial v_r/\partial r)$, $\dot{\gamma}_{\theta\theta} = 2(v_r/r)$, $\dot{\gamma}_{zr} = \dot{\gamma}_{rz} = (\partial v_r/\partial z)$ are calculated from eq. (10) and the remaining γ_{ij}'s are equal to zero. These were substituted into eq. (11), and the integral was solved using $h \ll a$. Simplification of the result gives

$$\frac{Q'}{N} = \frac{3\pi}{2}\eta a^2 \frac{h_0'^2}{h_0} \qquad (12)$$

The number of particle–particle interfaces is taken to be $N = 3N_p$, where N_p is the number of media particles in the mill chamber. This is related to the total mass of media M by

(13)

in which ρ_p is the density of the media particle. Equation (12) is then rewritten as

$$Q' = \frac{27}{\quad}\frac{M\eta}{\quad}\frac{h_0'^2}{\quad} \qquad (14)$$

$h_0'^2$ and h_0 in eq. (14) are unknown. Several reasonable approximations were made to proceed further with the analysis. The particle separation is assumed to be undergoing steady-state oscillations of amplitude ϵ at the mill angular frequency $\omega = 2\pi f$ about some average spacing $\bar{h}_0$, giving $h_0' = \epsilon\omega \sin(\omega t)$ and $h_0 = \bar{h}_0$ in eq. (14). Averaging over a rotational period provides the steady-state energy dissipation:

$$Q' = \frac{27\pi^2}{\quad}\frac{M\eta f^2}{\quad}\frac{\epsilon^2}{\quad} \qquad (15)$$

$$\dot{\gamma}_{rr}\Big|_{\max} = 2\frac{\partial v_r}{\partial r}\Big|_{\max} \approx -\frac{3}{4}\frac{h_0'}{h}\Big|_{\max} \approx -\frac{3\pi f}{2}\frac{\epsilon}{h}. \qquad (16)$$

Equations (15) and (16) are used to estimate the maximum extension rate for the typical test conditions $M = 0.142$ kg, $\rho_p = 5.5 \times 10^3$ kg/m^3, $a = 5 \times 10^{-4}$ m, $f = 2600$ rpm $= 43.3$ s^{-1}, $\eta \approx 1$ Pa-s, and $Q' = 1000$ W assuming 100% efficiency for conversion of electrical to mechanical energy. From eq. (15), $\epsilon^2/\bar{h}_0 = 0.15$ m. Substituting this result from the viscous dissipation into eq. (16) provides an estimate for the amplitude of the extension rate as a function of the average separation near $r \to 0$:

$$|\dot{\gamma}_{rr}|_{\max} \approx \frac{8.2 \times 10^4}{\sqrt{\bar{h}_0}}\ (\mathrm{s}^{-1}) \qquad (17)$$

with $\bar{h}_0$ in units of microns. The range of $|\dot{\gamma}_{rr}|$ for a realistic range of $\bar{h}_0$ is given in Table IV. Therefore, the maximum extension rate in the media mill is up to 5×10^6 s^{-1}.

Table IV The Maximum Extensional Component $|\dot{\gamma}_{rr}|$ for a Range of Average Particle Separation $\bar{h}_0$ at the Milling Conditions Used for the Test

$\bar{h}_0$ (μm)	$\lvert\dot{\gamma}_{rr}\rvert$ (s^{-1})
0.1	3.1×10^5
0.01	9.8×10^5
0.001	3.1×10^6
0.0005	4.4×10^6

Scission Mechanism

A small but detectable amount of chain scission took place during the milling. Since our method of fragment concentration on the polar media and the NMR detection are extremely sensitive to minute amounts of products, such small concentrations of scission products may have been undetected by investigators in the past. The complete range of scission products includes species that are small enough to evaporate at ambient conditions, and nonpolar species that remain soluble in the bulk of the polymer and are washed away by the FR solvent. This is summarized in Figure 8. Only those polar scission products that remained adsorbed on the milling media after the FR wash were extracted by the TFE solvent and identified.

The adsorbed scission product composition is compared with that of the initial polymers. The second column in Table I lists the backbone composition, and the third column is the end-group composition, with reference to the subscripts in the Experimental section. Since the composition of the backbone in the scission products is significantly different from the initial polymer, the scission is neither central nor by successive removal of the end groups for both the Y and Z polymers. The extracts from both polymers contained acid end groups and trifluoroacetic acid. This is consistent with disproportionation [eq. (5)]. It is also unlikely that free radicals [eq. (3)] or electrons [eq. (4)] would be stable in such a nonpolar environment. The composition of the detected fragments (second column in Table I) seems to differ from that of the initial polymer in a way that is consistent with scission occurring predominantly at certain groups, as will be discussed below.

The primary scission reactions consistent with the observed products are reactions I, III, and IV in Figure 9. Hydrolysis of the scission products is shown by reactions II and V in Figure 9. R, R′, R″, and M are portions of the polymer chain that are not affected by the scission event.

The source of the $CF_3CFO_2^-$ as described above is straightforward and objectively determined from the initial polymer composition. Interpretation of the fragment backbone composition data is more qualitatively described below by comparison with the initial composition of the polymer backbone to investigate the scission mechanism. The initial Y polymer backbone consists, on the average, of 95.7/(3.3 + 1.0) = 22 of $-OCF(CF_3)CF_2O-$ groups for each $\{-OCF_2O-$ or $-OCF(CF_3)O-\}$ group. The extract consists of five to seven $-OCF(CF_3)CF_2O-$ groups [including the $-OCF(CF_3)CO_2^-$ ends]. Thus, the products found

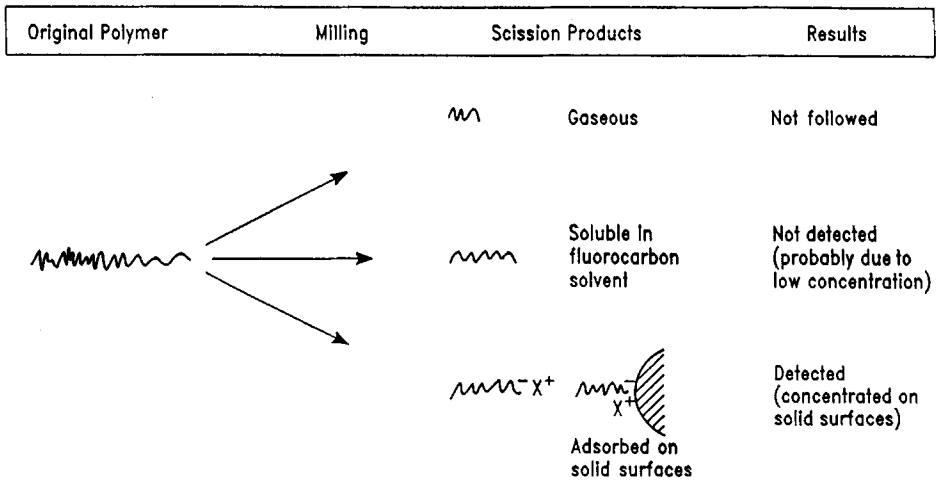

Figure 8 An illustration of the scission products' pathway, showing that only a portion of the fragments are detected by the solvent-extraction technique.

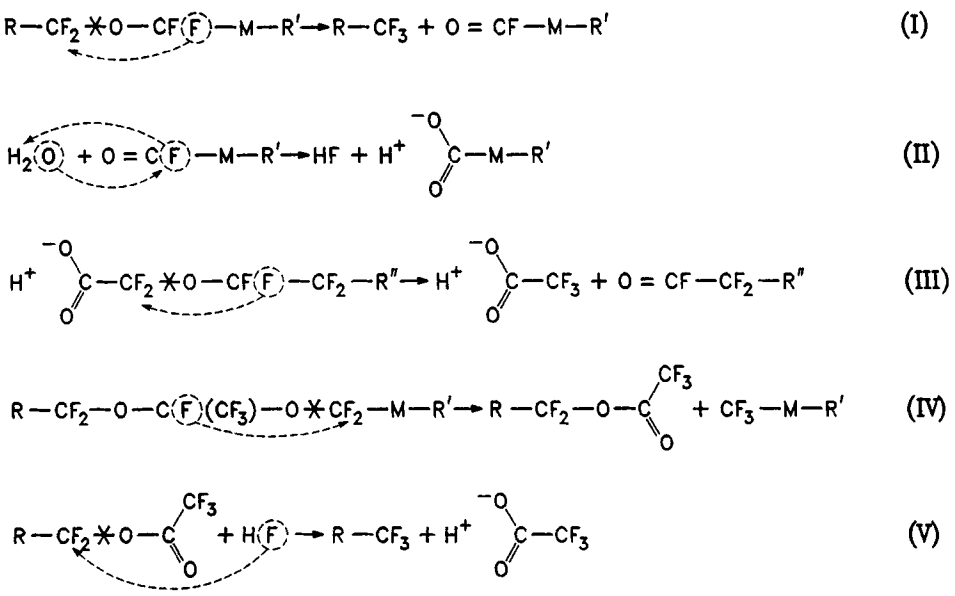

Figure 9 Chemical reaction steps involved in the chain scission and hydrolysis of scission products. Scissioned bonds are indicated by the X.

in the extract were not derived from the average region of the polymer chain. Scission occurred primarily where there were five to seven $-OCF(CF_3)CFO-$ groups surrounded by $-OCF_2O-$ or $-OCF(CF_3)O-$ groups.

The initial Z polymer had a ratio of odd-numbered units $\{-OCF_2O- + -OCF_2CF_2CF_2O-\}$ to even-numbered units $\{-OCF_2CF_2O- + -OCF_2CF_2CF_2O-\}$ of ≈ 1.79 that decreased to ≈ 0.46 in the extract. The most scission occurred at an odd-numbered unit with the acid end groups formed from the even-numbered unit and the other part remaining soluble.

For both polymers, in general, the mechanical scission due to hydrodynamic forces must occur at points along the chain where the shear stress is sufficiently concentrated to overcome the bond energy in a short enough time so that bonds are broken before the stress relaxation by segmental motions can take place.

CONCLUSIONS

Mechanochemical scission of Y and Z perfluoropolyethers in a media mill with estimated shear rates up to $5 \times 10^6\ s^{-1}$ has been shown. Scission products include volatile monomer, fragments soluble in fluorocarbon solvents, and fragments with polar end groups (Fig. 8). Only products in the last category were detected. The molecular weight and degree of polymerization of fragments adsorbed on the ZrO_2 media were significantly lower than the original polymers. $CF_3CO_2^-$ was produced from both Y and Z polymers. The Y polymer extract contained several unit sequences of $-OCF(CF_3CF_2O-$ with $-OCF(CF_3)CO_2^-$ or $-OCF(CF_3)CF_3$ end groups. The Z polymer extract contained 6-unit sequences with the ratio of the $-OCF_2CF_2O-$ to the $-OCF_2CF_2CF_2CF_2O-$ groups slightly lowered. The $-OCF_2O-$ group was reduced significantly below its concentration in the original polymer. The end groups of the Z polymer fragments were $-OCF_3$ and $-CF_2CO_2^-$. Scission observed here occurs for molecular weights that are much lower than anticipated based on literature values of critical molecular weights that are above 10,000 even for shear stresses in the $10^6\ s^{-1}$ range. Thermally degraded polymer left on catalytic surfaces has many of the same components as mechanically degraded polymer. It appears that the weakest bond breaks, and it does not matter whether the energy input is thermal, mechanical, or triboelectric.

We appreciate the assistance of and discussions with M. S. Jhon and T. M. Kwon at Carnegie Mellon University; J. R. Lyerla, P. S. Alexopoulos, and P. H. Kasai at the Almaden Research Center, IBM Research; and D. D. Saperstein, J. M. Burns, S. Ghaderi, and C. E. Hignite at IBM AdStar.

REFERENCES

1. D. Sianesi, V. Zamboni, R. Fontanelli, and M. Binaghi, *Wear,* **18,** 85–100 (1971).
2. K. J. L. Paciorek, R. H. Kratzer, J. Kaufman, and J. H. Nakahara, *J. Appl. Polym. Sci.,* **24**(6), 1397–1411 (1979).
3. P. H. Kasai, W. T. Tang, and P. Wheeler, *Appl. Surf. Sci.,* **51,** 201–211 (1991).
4. P. H. Kasai and P. Wheeler, *Appl. Surf. Sci.* **52,** 91–106 (1991).
5. P. H. Kasai, *Adv. Info. Storage Syst.,* **4,** 291–314 (1992).
6. S. Mori and W. Morales, *Tribol. Trans.,* **33**(3), 325–332 (1990).
7. V. J. Novotny, T. E. Karis, and N. W. Johnson, *J. Tribol.,* **114,** 61–67 (1992).
8. G. Marchionni, G. Ajroldi, P. Cinquina, E. Tampellini, and G. Pezzin, *Polym. Eng. Sci.,* **30**(14), 829–834 (1990).
9. J. A. Odell, A. Keller, and Y. Rabin, *J. Chem. Phys.,* **88**(6), 4022–4028 (1988).
10. J. A. Odell, A. J. Muller, A. N. Kwabena, and A. Keller, *Macromolecules,* **23,** 3092–3103 (1990).
11. Y. Rabin, *J. Chem. Phys.,* **86**(9), 5215–5216 (1987).
12. Y. Rabin, *J. Non-Newt. Fluid Mech.,* **30,** 119–123 (1988).
13. J. F. S. Yu, J. L. Zakin, and G. K. Patterson, *J. Appl. Polym. Sci.,* **23,** 2493–2512 (1979).
14. B. M. E. Van Der Hoff and V. K. Chopra, *J. Appl. Polym. Sci.,* **23,** 2373–2384 (1979).
15. S. H. Agarwal and R. S. Porter, *J. Appl. Polym. Sci.,* **25,** 173–185 (1980).
16. F. L. Buchholz and L. R. Wilson, *J. Appl. Polym. Sci.,* **32,** 5399–5413 (1986).
17. M. Netopilik, M. Kubin, G. Schultz, J. Vohlidal, I. Kossler, and P. Kratochvil, *J. Appl. Polym. Sci.,* **40,** 1115–1130 (1990).
18. I. Arvanitoyannis, J. M. V. Blanshard, and I. Kolokuris, *Polym. Int.* **27,** 7–15 (1992).
19. A. M. Basedow and K. H. Ebert, *Adv. in Polym. Sci.,* **22,** 83–148 (1976).
20. R. H. Perry and C. H. Chilton, *Chemical Engineers Handbook,* 5th ed., McGraw-Hill, New York, 1973.
21. R. B. Bird, R. C. Armstrong, and O. Hassager, *Dynamics of Polymeric Liquids,* Wiley, New York, 1977, Vol. 1.

Received February 2, 1993
Accepted April 15, 1993